Energy Equip. Sys./ Vol. 11/No. 2/June 2023/ 165-191

ENERGY EQUIPSYS

Energy Equipment and Systems
http://energyequipsys.ut.ac.ir
www.energyequipsys.com

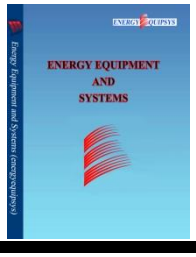

Comparative analysis of a novel geothermal and nanofluid-based solar-driven multigeneration system integrated with high-temperature Kalina cycle: Energy, Exergy, and exergo-economics (3E) analysis

Authors
Amin Habibzadeh[a]
Majid Abbasalizadeh[a*]
Iraj Mirzaee[a]
Samad Jafarmadar[a]
Hassan Shirvani[b]

[a] Department of Mechanical Engineering, Engineering Faculty, Urmia University, Urmia,Iran

[b] Faculty of Science and Engineering, Anglia Ruskin University, Chelmsford, UK

Article history:

Received : 4 October 2022
Accepted : 10 January 2023

ABSTRACT

In this comparative study, the thermodynamic and economic investigation of an integrated system driven by a parabolic trough collector and geothermal water is carried out. The proposed multigeneration system is composed of a high-temperature modified Kalina cycle, an electrolyzer, a combined organic Rankine cycle-ejector refrigeration (ORC-EJR) cycle, a reverse osmosis (RO) desalination unit, and a domestic water heater. The absorption fluids applied in the solar collector are AL_2O_3 and CuO-based nanofluids, and Therminol VP1 as the base fluid. A comprehensive thermodynamic and exergo-economic analysis is carried out for the proposed cycle. Engineering Equation Solver (EES) software is used in all conducted simulations. Nanoparticle percentage, solar irradiation, ambient temperature, and collector inlet temperature were the parameters studied to find their effects on the hydrogen production rate, total net power, useful energy achieved, energy and exergy efficiency, collector outlet temperature, and freshwater production rate. The highest outlet temperature of the solar collector was found to be 688.7 K, and the maximum energetic and exergetic efficiencies of the cycle were 34.45% and 17.25%, respectively. The exergo-economic outputs show that the PEM with 1.99 $/h has the maximum exergy destruction cost rate. The results depicted that CuO-based nanofluid has better performance from the exergy and exergo-economic viewpoints compared to AL_2O_3-nanofluid. Also, the results proved that the nanoparticle percentage and solar irradiation increases lead to the increase in hydrogen production rate and total net power produced by the system. Moreover, the freshwater production rate increases when the ambient temperature and the collector inlet temperature rise.

Keywords: Thermodynamic analysis, PTC, geothermal, multigeneration system, nanofluids.

1. Introduction

In recent years, one of the major worries of society is the rapid declining non-renewable fossil fuel reserves, world population growth, environmental pollution, as well as growing energy demand [1]. This concern has led energy sector planners to use more environment-friendly and more efficient systems and replace centralized power plants with new power generation methods [2]. One of the basic strategies to reach these goals is to use multigeneration systems. In multigeneration systems, in addition to providing electrical

* Corresponding author: Majid Abbasalizadeh
Department of Mechanical Engineering, Engineering Faculty, Urmia University, Urmia,Iran
Email: m.abbasalizadeh@urmia.ac.ir

power, waste heat can be used to meet various needs, including the production of cooling, heating, drinking water, and hot water [3]. Utilizing this technology, due to the reduction of many losses that occur when converting thermal energy into mechanical or electrical, can not only significantly increase efficiency but also reduce environmental impact and overall system costs [4].

Numerous investigations have been accomplished in the field of exergy-economic modeling and analysis of multigeneration cycles. Al-Ali and Dincer [5] proposed a novel geothermal-solar system producing power, cooling, heating, heat, and hot water. The results showed a 60% and 10% difference between energy and exergy efficiencies when considering sole generation and the proposed multigeneration system. Panchal et al. [6] studied the integrated solar-geothermal cycle, including the Rankine cycle, absorption chiller cycle, and drying process in residential applications. The effects of different parameters were investigated to show the system performance variations. The results cleared that the overall efficiency of the multigeneration cycle is much higher than the single production cycle. A thermo-economic analysis is carried out by Khalid et al. [7] for a renewable energy-based multigeneration system to produce power, hot water, hydrogen, cooling, and heating. The proposed cycle was capable of producing 2.7 kg/h of hydrogen. Moreover, the levelized cost of electricity was discovered to be 0.089 $/kWh. Waseem et al. [8] analyzed a solar-geothermal multigeneration system producing hydrogen, power, and cooling. The proposed cycle included an electrolyzer, Rankine cycle, and vapor absorption cycle. Two arrangements were comparatively investigated, and a 0.45% power efficiency difference was observed. Li et al. [9] developed a system including a geothermal cycle, solar cycle, and PEM system. The system generated electricity, hydrogen, heating, and hot water. To find the irreversibilities, energy, and exergy analyses were done. Compared to the sole geothermal system, the proposed system can produce 148.3% more power. A novel multigeneration solar-geothermal system producing electricity for a living area was introduced by Sen et al. [10]. The presented system could generate 2900kW electricity and 0.0185 kg/s hydrogen. The thermodynamic analysis made it clear that the energy and exergy efficiencies of the cycle were 5.90% and 18.99%, respectively. Atiz [11] investigated an integrated solar-geothermal system for electricity and hydrogen production purposes. The effects of three different solar collectors including parabolic trough solar collectors (PTSCs), evacuated tube solar collectors (ETSCs), and flat plate solar collectors (FPSCs) were studied and compared on the performance of the system. The results showed that the temperature of the geothermal resource is increased by solar collectors as well as the overall energy and exergy efficiencies. The integrated system could produce 414.93 MJ of electricity and 2758.69 g of hydrogen in a day. Sohani et al. [12] studied the effects of price inflation on the optimal performance of a solar-geothermal system capable of combined production of hydrogen, power, freshwater, and heat. The results indicated that when inflation rises from 0.05 to 0.20, annual freshwater production drops by 15 % while annual freshwater increases by 12 %. By increasing inflation, the payback period increases from 6.11 to 7.39 years showing the economic viability of such a combined solar-geothermal system. A solar-driven multi-production system of power, cooling, and hydrogen generation was developed and exergetically assessed by Ghorbani et al. [13]. According to the results, the overall energy and exergy efficiencies were 90.77 % and 92.19 %, respectively. The proposed hybrid system produced 4.36 MW power, 1.65 MW cooling, and 2026 kg/h hydrogen. Mahmoudan et al. [14] investigated a novel multigeneration system driven by geothermal and solar energy. The integrated system was composed of parabolic trough collectors, a Kalina cycle, an ejector refrigeration system, a thermoelectric generator (TEG) unit, an organic Rankine cycle, and a PEM electrolyzer to produce electricity, domestic hot water, a cooling load, and hydrogen. Optimal exergy efficiency, total product cost, and hydrogen production rate were calculated to be 35.2%, 37.8 $/GJ, and 1.9 kg/h, respectively. A parametric study indicated that applying the TEG unit would enhance system performance. Hashemian and Noorpoor [15] proposed a novel geothermal-biomass-powered

multi-generation system through thermo-economic-environmental aspects. The system applied the Rankine cycle, a dual-effect absorption refrigeration unit, a proton exchange membrane water electrolyzer, and a biomass combustor to produce electricity, heating, cooling, as well as hydrogen and freshwater. They showed that the studied system provided 31.68 MW direct power, 23.3 m3/h freshwaters, and 88.12 kg/h hydrogen, and energetic and exergetic efficiencies were calculated to be 58.54% and 16.45%. Moreover, the total product cost rate was attained at 1.629 $/s and the exergo-environmental impact factor was found to be 0.9.

The maximum temperature that can be produced by a parabolic trough solar collector (PTC) is 400°C with oil and 550°C with salt [16]. One of the ways to reach better and higher performance in PTC is by transferring more useful heat to the working fluid by using nanofluids [17]. Several studies considered the use of different nanofluids in PTCs. Subramani et al. [18] studied the thermal efficiency of a solar PTC collector applying Al2O3/DI-H2O nanofluids in different concentrations, mass flows, and turbulent regimes. The results showed that by using nanofluid compared with pure water, the efficiency of the collector increased up to 56%. The thermodynamic analysis of a PTC receiver tube using oil–Al2O3 nanofluid with a concentration ratio of 86 was investigated by Mwesigye et al. [19] applying the entropy generation minimization method. The authors proved that by varying the nanofluid temperature from 350 to 600 K, the thermal efficiency of the PTC increased by up to 7.6%. The volume fraction rising led to a reduction in the optimal Reynolds number. In a comparative study, Bellos et al. [20] studied the effect of using three working fluids including thermal oil, thermal oil with nanoparticles, and pressurized water as well as geometry on the thermal efficiency enhancement of the parabolic collector. According to the final results, nanofluid use increased the collector efficiency up to 4.25% while this amount is 4.55% for geometry. Wang et al. [21] investigated the application of Al2O3/synthetic oil nanofluid on the performance of the parabolic trough collector systems. The effects of different parameters on the performance of the PTC were studied. It is discovered that by using the nanofluid, higher efficiencies could achieve and the temperature gradients and the maximum temperature in the absorber were decreased. Furthermore, the varying temperature and DNI caused a reduction in the inlet temperature and the inlet velocity. The comparison of applying Al_2O_3 and Fe_2O_3-based nanofluids in a parabolic trough solar collector and a parabolic dish solar collector was studied by Abid et al. [22]. The collectors were combined with a Rankine cycle and an electrolyzer to produce electricity and hydrogen. According to the results, the power obtained by the system using a parabolic dish collector is higher than the system using a parabolic trough collector. Compared to the base fluids, applying nanofluids leads to higher power production and better efficiency. Moreover, more hydrogen could be produced when nanofluids were utilized. Ratlamwala et al. [23] studied a solar-geothermal multigeneration system generating power, hydrogen, cooling, hot water, and freshwater. Al_2O_3 and Fe_2O_3 nanofluids were applied in the solar part of the proposed cycle. According to the results, both of the nanofluids showed excellent heat transfer properties, but Al_2O_3-based nanofluid resulted in better performance compared with Fe_2O_3-based nanofluid. Furthermore, when the nanoparticle percentage increased, the amount of power and hydrogen rate production decreased. Bellos et al. [24] surveyed the thermal increment of parabolic trough collectors when the Syltherm 800/Cu nanofluid was applied. The investigation of three different collectors revealed that for cermet coating and 25L/min flow rate, the amount of increment for the bare tube was 7.16%, for the non-evacuated receiver was 4.87% and for the evacuated receiver was 4.06%. Khan et al. [25] studied the effect of applying nanofluids in a solar-based cycle from energy, exergy, and exergo-environmental point of view. The influence of three nanofluids, including Fe2O3/Therminol VP1, SiO2/Therminol VP1, and Cu/Therminol VP1, were compared by considering different parameters. The results showed that among the studied nanofluids, SiO2/VP1 presented better outcomes. Moreover, the amount of CO2 was reduced for all the studied nanofluids.

Increasing nanoparticle concentration leads to an increment in the exergy efficiency and a decrease in the nanoparticle thermal conductivity. Ibrahim and Kayfeci [26] studied using two kinds of nanofluids in a parabolic trough solar collector of a trigeneration system. The results showed that by using ferrofluid and graphene as the nanoparticles, the overall performance of the proposed system improved. Graphene nanoparticles indicated better performance in comparison with ferrofluid nanoparticles. Allouhi et al. [27] studied the effect of using different nanoparticles for medium and high-temperature PTCs mathematically. They concluded that high operating temperatures are more appropriate for using nanofluids in PTCs as higher gains of energy are achieved. The maximum exergy efficiency of CuO-based nanofluid was calculated to be about 9.05%. Kalbande et al. [28] studied the possibility of attaining a higher temperature range of above 200°C in oil-based thermal energy storage systems. They used aluminum oxide (Al2O3) and soybean oil nanofluid as the heat transfer fluid to store and transfer the sensible heat. After a mathematical analysis, they could achieve up to 220°C in a parabolic trough solar collector coupled with a thermal storage system. Tonekaboni et al. [29] studied the amount of enhancement of the solar collectors by adding porous media and nanofluid. They applied 90% porosity copper, CuO, and Al2O3 nanofluids to investigate the changing in the thermal properties of different types of solar collectors. The results showed that adding porous media and nano-fluids increased an average of 14.4% collector energy efficiency and 8.08% collector exergy efficiency. Moreover, the highest amount of energy and exergy efficiencies were 60.12% and 18.84%, respectively which were obtained for parabolic solar collectors. Said et al. [30] surveyed a nanofluid-based parabolic trough collector from energy, exergy, economic, and environmental points of view. The results showed that by adding Ti3C2 to the silicon oil, the thermal conductivity of the nanofluid enhances from 70 % to 89%. It is found that, compared to pure oil, applying nanofluid reduces the system's cost by 0.021M$ and increases the gained energy by 1.51%. For energy analysis, the annual CO2 reduction varies from 2.25 to 2.30 tons CO2/year.

According to the literature review, there is a great concern about applying the nanofluid in parabolic trough solar collectors. On the other hand, publications investigating the effects of nanofluids in high-temperature PTCs are rare. Moreover, to the best knowledge of the authors, there is no study of the combination of high-temperature Kalina cycle and nanofluid applied parabolic trough solar collectors. In this research a novel multigeneration system including solar and geothermal energy sources where Al2O3–based and CuO–based nanofluids were used as working fluids in PTC. The proposed system contains a high-temperature modified Kalina cycle, an electrolyzer, a combined ORC-EJR cycle, an RO desalination unit, and a domestic water heater.

A summary of the main goals and novelties of this research is presented below:

- Introducing a new multigeneration energy system using solar and geothermal renewable sources.
- Applying a modified high-temperature Kalina cycle for retrieving the solar source energy.
- Presenting the overall performance of the proposed novel multigeneration system.
- Energy, exergy, and exergo-economic analysis of the proposed systems are applied to perform a comprehensive evaluation of the system.
- Comparing the use of three working fluids to analyze the performance of the system.
- Producing hydrogen and fresh water from the novel energy system.

NOMENCLATURE

A	Area (m2)
c	Cost per exergy unit ($/GJ)
$\dot{C}$	Cost rate ($/h)
C_p	Specific heat capacity (J/kgK)
CRF	Capital recovery factor
$cooling$	Cooling
con	Condenser
D	Destroyed
DWH	Domestic water heater
eje	Ejector
$electric$	Electricity

eva	Evaporator
exv	Expansion valve
E	Energy input (kW)
Ex	Exergy rate (W)
F	Faraday constant (C/mol)
f_k	Exergoeconomic factor (%)
F_1	Collector efficiency factor
F_R	Heat transfer factor
f	Feed water
H_2	Hydrogen
H_2O	Water
HX	Heat exchanger
in	Inlet
G_b	Solar irradiation (W/m2)
h	Heat transfer coefficient (W/m2K)
J	Current density (A/m2)
J_0	Exchange current density (A/m2)
J_a^{ref}	Pre - exponential factor (A/m2)
K	The ratio of specific heats (CP/CV)
k	Thermal conductivity (W/m K)
L	Collector length (m)
M	Molecular weight (kg/mol)
m	Mass flow rate (kg/s)
N_x	Outlet flow rate of fluid x (kg/s)
n_{cs}	Number of collectors in series
n_{cp}	Number of collectors in parallels
P	Pressure (bar)
Q	Heat transfer rate (W)
Q_u	Useful energy gain
R	Overall ohmic resistance
RR	Recovery ratio
r_k	Relative cost difference (%)
S	Absorbed solar radiation
T	Temperature (K)
TCF	Temperature correction factor
U_L	Solar collector's overall heat loss coefficient
V	Overpotential (V)
V_0	Reversible potential (V)
V_{ohm}	Ohmic overpotential of the electrolyte (V)
W	Net output power (kW)
w	Collector width (m)
X	Salt concentration (g/kg)
Z	The capital cost of a component ($)
$\dot{Z}$	Capital cost rate ($/h)

Subscripts

0	Ambient
$1,2,...$	State points
a	Anode
act	Activation
ap	Aperture
avg	Average
bf	Base fluid
c	Cathode
ch	Chemical
k	Kth component
KAL	Kalina
mx	Mixer
net	net
nf	nanofluid
np	nanoparticle
out	Outlet
p	Pump
PEM	Proton exchange membrane
ph	Physical
prh	Preheater
PTC	Parabolic trough collector
r	Receiver tube
re	Recuperator
$reacted$	Entering water of PEM electrolyzer
r,i	Receiver inlet
r,o	Receiver outlet
RO	Reverse osmosis
$ORC-EJR$	Organic Rankine Cycle-Ejector Refrigeration cycle
sep	Separator
spl	Splitter
sun	sun
t	Turbine
th	Thermal
vg	Vapor generator
w	Work

Greek Symbols

α	Absorptivity of receiver
γ	Correction factor for diffuse radiation
$\sigma(x)$	Ionic conductivity of the membrane
η	Efficiency
μ	Dynamic Viscosity
$\lambda(x)$	Water content at location x
ρ	Density (kg/m3)
τ_c	Transmissivity of the cover glazing

τ_p	Effective transmissivity of the parabolic trough collector
ϕ	Nanoparticle volume concentration

2. System description

Figure 1 presents the schematic of the considered multigeneration system. As is shown, the principal components of the system are a low-temperature geothermal source, a nanofluid solar system-based modified Kalina system, an RO desalination unit, a combined ORC-EJR cycle, a PEM electrolyzer, and a domestic water heater. The outcomes of the proposed system are electricity, fresh water, hydrogen, hot water, heating, and cooling. The primary energy sources of the system are geothermal and solar cycles. The solar cycle employed in this system has two main functions: to act as the high-temperature energy source of the Kalina cycle and to increase the temperature of the flow extracted from the ground. The parabolic trough collector absorbs energy by applying Al_2O_3, and CuO nanoparticles added to the Therminol_VP1 as the base fluid. The geothermal water, after gaining energy from the heat exchanger of the solar system, first enters the vapor generator of the combined ORC-EJR cycle to supply the cycle's energy needed to produce power. Then, it discharges into the reinjection well, passing the domestic water heater, which produces hot water. The generated power in the modified Kalina cycle is used as the electricity in the residential area and the source power of the RO desalination unit to purify the sea water and supply fresh water. The combined ORC-EJR cycle produces a cooling effect and power. The power generated in the combined ORC-EJR cycle is divided into two streams: employed in the residential area and applied in the PEM electrolyzer to produce hydrogen.

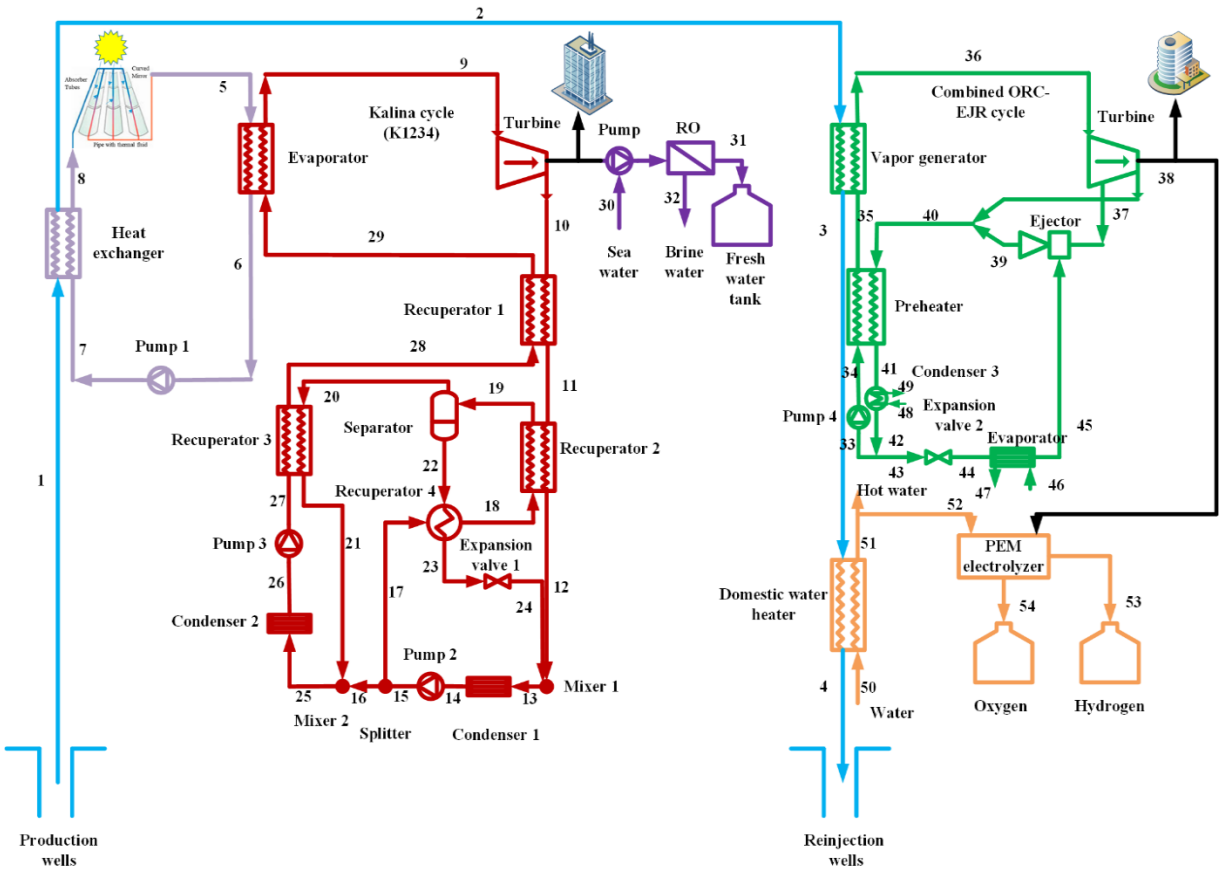

Fig. 1. Schematic diagram of the proposed multigeneration energy system

3. Mathematical modeling

The mathematical simulation evaluates the performance, energy, and exergy efficiency, and exergy destruction rate of the system. Engineering Equation Solver (EES) [31] was used to determine the properties of the working fluids and solve the relations of all components of the system. For simplifying the modeling process, some considerations are taken as follows [32,33]:

- The system functions under steady-state conditions.
- The changes in potential and kinetic energies, as well as pressure losses in the pipes and heat exchangers, are ignored.
- All turbines, pumps, condensers, and valves are assumed adiabatic systems.
- The outlet streams of the condensers and evaporators are considered to be saturated liquid and saturated vapor, respectively.
- Isentropic efficiency is assumed for pumps and turbines.
- Solar irradiation is presumed to be uniform and steady-state.
- Geothermal hot water is considered to be net water with no pollution.

To model the multigeneration cycle, the primary input and design values are exhibited in Table 1.

Table 1. The input parameters for the modeling of the present study

Parameters	Unit	Value
GEOTHERMAL [34,35]		
Production well temperature, T_1	$(^{\circ}C)$	120
Production well Pressure, P_1	(bar)	7
SOLAR [36-38]		
Collector width, W	(m)	5.76
Collector length, L	(m)	12.27
Receiver outside diameter, $D_{o,r}$	(m)	0.07
Receiver inside diameter, $D_{i,r}$	(m)	0.066
Collector heat loss coefficient, U_L	$\left(\frac{W}{m^2 \cdot C}\right)$	3.82
Receiver inlet temperature, T_{ri}	$(^{\circ}C)$	180
The heat transfer coefficient inside the receiver, h_{fi}	$\left(\frac{W}{m^2 \cdot C}\right)$	300
The thermal conductivity of the receiver, K	$\left(\frac{W}{m^2 \cdot C}\right)$	16
Solar radiation intensity, G_b	$\left(\frac{W}{m^2}\right)$	850
Cover glazing transmissivity, τ_c	-	0.96
PTC effective transmissivity, τ_p	-	0.94
Receiver absorptivity, α_r	-	0.96
Correction factor for diffuse radiation, γ	-	0.95
KALINA [39]		
Turbine inlet ammonia concentration, x_9	-	0.49
Turbine inlet temperature, T_9	$(^{\circ}C)$	330
Turbine inlet pressure, P_9	(bar)	120
RO [40,41]		
Recovery ratio, RR	-	0.3
Number of elements, n_e	-	7
Number of pressure vessels, n_v	-	42
Seawater salinity, X_f	$\left(\frac{g}{kg}\right)$	43
ORC-EJR [42-44]		
Working fluid	Isopentane	
Turbine inlet pressure, P_{36}	(bar)	6.5
Evaporator temperature, T_{44}	$(^{\circ}C)$	−5

3.1.Energy and exergy analysis

The main conservation equations, mass, and energy, employed in analyzing the proposed system are as follows [45]:

$$\sum \dot{m}_{in} = \sum \dot{m}_{out} \quad (1)$$

$$\sum (\dot{m}h)_{out} - \sum (\dot{m}h)_{in} = Q - W \quad (2)$$

$$Ex = Ex_{ph} + Ex_{ch} \quad (3)$$

$$Ex_{ph} = \sum m_{in}\left[(h_{in} - h_{out}) - T_o(s_{in} - s_{out})\right] \quad (4)$$

$$Ex_{ch} = m_{in}\left[\left(\frac{x}{M_{NH3}}\right)ex^{o}_{ch,NH3} + \left(\frac{1-x}{M_{H_2O}}\right)ex^{o}_{ch,H_2O}\right] \quad (5)$$

In the above-mentioned equations, x is the molar fraction of ammonia, and *ch* and *ph* represent the chemical, and physical exergy, respectively.

By employing the energy and exergy balance relations for the multigeneration system, the transferred heat and power, and exergy destruction rate of each component can be computed as listed in Table 2.

Table 2. Energy conservation and exergy destruction rate relations for the plant's elements

Component	Energy balance equations	Exergy destruction rate equations
PTC field	$m_8h_8 + Q_u = m_5h_5$	$Ex_{D,PTC} = Ex_{sun} + Ex_8 - Ex_5$
Heat exchanger	$Q_{HX} = m_1(h_2 - h_1) = m_7(h_7 - h_8)$	$Ex_{D,HX} = Ex_1 + Ex_7 - Ex_2 - Ex_8$
Kalina evaporator	$Q_{eva,KAL} = m_5(h_5 - h_6) = m_9(h_9 - h_{29})$	$Ex_{D,eva,KAL} = Ex_5 + Ex_{29} - Ex_6 - Ex_9$
Kalina turbine	$\dot{W}_{t,KAL} = m_9(h_9 - h_{10})$	$Ex_{D,t,KAL} = Ex_9 - \dot{W}_{t,KAL} - Ex_{10}$
Kalina recuperator 1	$Q_{re1,KAL} = m_{10}(h_{10} - h_{11}) = m_{28}(h_{29} - h_{28})$	$Ex_{D,re1,KAL} = Ex_{10} + Ex_{28} - Ex_{11} - Ex_{29}$
Kalina recuperator 2	$Q_{re2,KAL} = m_{11}(h_{11} - h_{12}) = m_{18}(h_{19} - h_{18})$	$Ex_{D,re2,KAL} = Ex_{11} + Ex_{18} - Ex_{12} - Ex_{19}$
Kalina recuperator 3	$Q_{re3,KAL} = m_{20}(h_{20} - h_{21}) = m_{27}(h_{28} - h_{27})$	$Ex_{D,re3,KAL} = Ex_{20} + Ex_{27} - Ex_{21} - Ex_{28}$
Kalina recuperator 4	$Q_{re4,KAL} = m_{17}(h_{17} - h_{18}) = m_{22}(h_{23} - h_{22})$	$Ex_{D,re4,KAL} = Ex_{17} + Ex_{22} - Ex_{18} - Ex_{23}$
Kalina mixer 1	$m_{12}h_{12} + m_{24}h_{24} = m_{13}h_{13}$	$Ex_{D,mx1,KAL} = Ex_{12} + Ex_{24} - Ex_{13}$
Kalina mixer 2	$m_{16}h_{16} + m_{21}h_{21} = m_{25}h_{25}$	$Ex_{D,mx2,KAL} = Ex_{16} + Ex_{21} - Ex_{25}$
Kalina condenser 1	$Q_{con1,KAL} = m_{13}(h_{13} - h_{14})$	$Ex_{D,con1,KAL} = Ex_{13} - Ex_{14} - Q_{con1,KAL}\left(1 - \frac{T_0}{T_{14}}\right)$
Kalina condenser 2	$Q_{con2,KAL} = m_{25}(h_{25} - h_{26})$	$Ex_{D,con2,KAL} = Ex_{25} - Ex_{26} - Q_{con2,KAL}\left(1 - \frac{T_0}{T_{26}}\right)$
Kalina pump 2	$\dot{W}_{p2,KAL} = m_{14}(h_{15} - h_{14})$	$Ex_{D,p2,KAL} = \dot{W}_{p2,KAL} + Ex_{14} - Ex_{15}$
Kalina pump 3	$\dot{W}_{p3,KAL} = m_{26}(h_{27} - h_{26})$	$Ex_{D,p3,KAL} = \dot{W}_{p3,KAL} + Ex_{26} - Ex_{27}$
Kalina splitter	$m_{15}h_{15} = m_{16}h_{16} + m_{17}h_{17}$	$Ex_{D,spl,KAL} = Ex_{15} - Ex_{16} - Ex_{17}$
Kalina separator	$m_{19}h_{19} = m_{20}h_{20} + m_{22}h_{22}$	$Ex_{D,sep,KAL} = Ex_{19} - Ex_{20} - Ex_{22}$
Kalina expansion valve 1	$h_{23} = h_{24}$	$Ex_{D,exv1,KAL} = Ex_{23} - Ex_{24}$
ORC vapor generator	$Q_{vg,ORC-ERC} = m_2(h_2 - h_3) = m_{35}(h_{36} - h_{35})$	$Ex_{D,vg,ORC-ERC} = Ex_2 + Ex_{35} - Ex_3 - Ex_{36}$
ORC turbine	$\dot{W}_{t,ORC-ERC} = m_{36}(h_{36} - h_{37}) + m_{38}(h_{37} - h_{38})$	$Ex_{D,t,ORC-ERC} = Ex_{36} - \dot{W}_{t,ORC-ERC} - Ex_{37} - Ex_{38}$
ORC ejector	$\mu_{eje} = \frac{m_{45}}{m_{37}}$	$Ex_{D,eje,ORC-ERC} = Ex_{37} + Ex_{45} - Ex_{39}$
ORC preheater	$Q_{prh,ORC-ERC} = m_{34}(h_{35} - h_{34}) = m_{40}(h_{40} - h_{41})$	$Ex_{D,prh,ORC-ERC} = Ex_{34} + Ex_{40} - Ex_{35} - Ex_{41}$
ORC pump 4	$\dot{W}_{p,ORC-ERC} = m_{33}(h_{34} - h_{33})$	$Ex_{D,p4,ORC-ERC} = \dot{W}_{p4,ORC-ERC} - Ex_{33} + Ex_{34}$
ORC condenser 3	$Q_{con3,ORC-ERC} = m_{41}(h_{41} - h_{42}) = m_{48}(h_{49} - h_{48})$	$Ex_{D,con3,ORC-ERC} = Ex_{41} + Ex_{48} - Ex_{42} - Ex_{49}$
ORC expansion valve 2	$h_{43} = h_{44}$	$Ex_{D,exv2,ORC-ERC} = Ex_{43} - Ex_{44}$
ORC evaporator	$Q_{eva,ORC-ERC} = m_{44}(h_{45} - h_{44})$	$Ex_{D,EV,ORC-ERC} = Ex_{44} + Ex_{46} - Ex_{45} - Ex_{47}$
PEM	$\dot{W}_{PEM} = (m_{52}h_{52} - m_{53}h_{53} - m_{54}h_{54})$	$Ex_{D,PEM} = Ex_{52} + \dot{W}_{PEM} - Ex_{53} - Ex_{54}$
DWH	$Q_{DWH} = m_3(h_3 - h_4) = m_{50}(h_{51} - h_{50})$	$Ex_{DWH} = Ex_3 + Ex_{50} - Ex_4 - Ex_{51}$
RO	$\dot{W}_{RO} = (m_{30}h_{30} - m_{31}h_{31} - m_{32}h_{32})$	$Ex_{D,RO} = Ex_{30} - Ex_{31} - Ex_{32}$

The equations used for the simulation of the RO unit and PEM electrolyzer are expressed in Tables 3 and 4, respectively.

3.2. Calculation of nanofluid heat transfer properties

In this study, Al_2O_3 and CuO nanoparticles have been applied inside Therminol_VP1 as the base fluid. The thermal properties of the nanoparticles are presented in Table 5.

Compared to the base fluids, the nanofluids offer different thermal properties, which can be calculated by the following formulas, applying the properties of the nanoparticles (*np*) and the base fluid (*bf*).

The density of the nanofluid (ρ) is presented as [49]:

$$\rho_{nf} = \varphi.\rho_{np} + (1-\varphi).\rho_{bf} \quad (6)$$

in which φ is the volume concentration of the nanoparticle.

Table 3. RO unit required modeling relations [46]

The recovery ratio	$RR = \frac{\dot{m}_{31}}{\dot{m}_{30}}$
Saline water flow rate	$\dot{m}_{32} = \dot{m}_{30} - \dot{m}_{31}$
Osmotic pressure	$P_{net} = P_{avg,f} - 75.85 \times X_{31}$
Average Osmosis pressure	$P_{avg,f} = \frac{P_{30}+P_{32}}{2} = 37.92 \times (X_{30} + X_{32})$
Temperature correction factor	$TCF = \exp\left\{2700 \times \left(\frac{1}{T+273} - \frac{1}{298}\right)\right\}$
Membrane water permeability	$K_w = \frac{6.84 \times 10^{-8} \times (18.6865 - 0.177 \times X_{32})}{(T+273)}$
High-pressure pump power	$W_{p,RO} = \frac{\dot{m}_{30} \times \Delta P}{\rho_{30} \times \eta_p}$

Table 4. PEM electrolyzer required modeling relations [47]

Electrical energy consumption	$E_{electric} = JV$
Electrolyzer voltage	$V = V_0 + V_{act,c} + V_{act,a} + V_{ohm}$
Reversible equation	$V_0 = 1.229 - 0.00085(T_{PEM} - 298)$
Activation overpotential	$A_{act,i} = \frac{RT}{F}\sinh^{-1}\left(\frac{J}{2J_{0,i}}\right) = J_a^{ref}\exp\left(\frac{-E_{act,i}}{RT}\right), i = a,c$
Ohmic overpotential	$V_{ohm} = JR_{PEM}, R_{PEM} = \int_0^L \frac{dx}{\sigma[\lambda(x)]}, \lambda(x) = \frac{\lambda_a - \lambda_c}{D}x + \lambda_c$ $\sigma[\lambda(x)] = [0.5139\lambda(x) - 0.326]\exp\left[1268\left(\frac{1}{303} - \frac{1}{T}\right)\right]$
Rate of produced H_2	$N_{H_2,Out} = \frac{J}{2F} = N_{H_2O,reacted}$

Table 5. Properties of the studied nanoparticles [48]

Particle	ρ (kg/m^3)	k (W/mK)	c_p (kJ/kgK)
Al_2O_3	3970	40	0.765
CuO	6320	77	0.532

The specific heat capacity of the nanofluid (C_p) can be expressed as [50]:

$$c_{p,nf} = \frac{\rho_{np}.\varphi.c_{p,np} + \rho_{bf}.(1-\varphi).c_{p,bf}}{\rho_{nf}} \quad (7)$$

The nanofluid thermal conductivity (k) is calculated as [51]:

$$k_{nf} = k_{bf}.\frac{k_{np} + 2k_{bf} + 2(k_{np} - k_{bf}).(1+\beta)^3.\varphi}{k_{np} + 2k_{bf} - (k_{np} - k_{bf}).(1+\beta)^3.\varphi} \quad (8)$$

In equation (8), β is defined as the nanolayer thickness to the original particle radius and usually is taken as 0.1 [52].

The dynamic viscosity of the nanoparticle (μ) is estimated by the following correlation [53]:

$$\mu_{nf} = \mu_{bf}.(1 + 2.5\varphi + 6.5\varphi^2) \quad (9)$$

The thermal properties of the nanofluids are displayed in Fig. 2. In the following figures, the properties, including the density, the specific heat capacity, and the thermal conductivity, are presented for different nanoparticle concentrations.

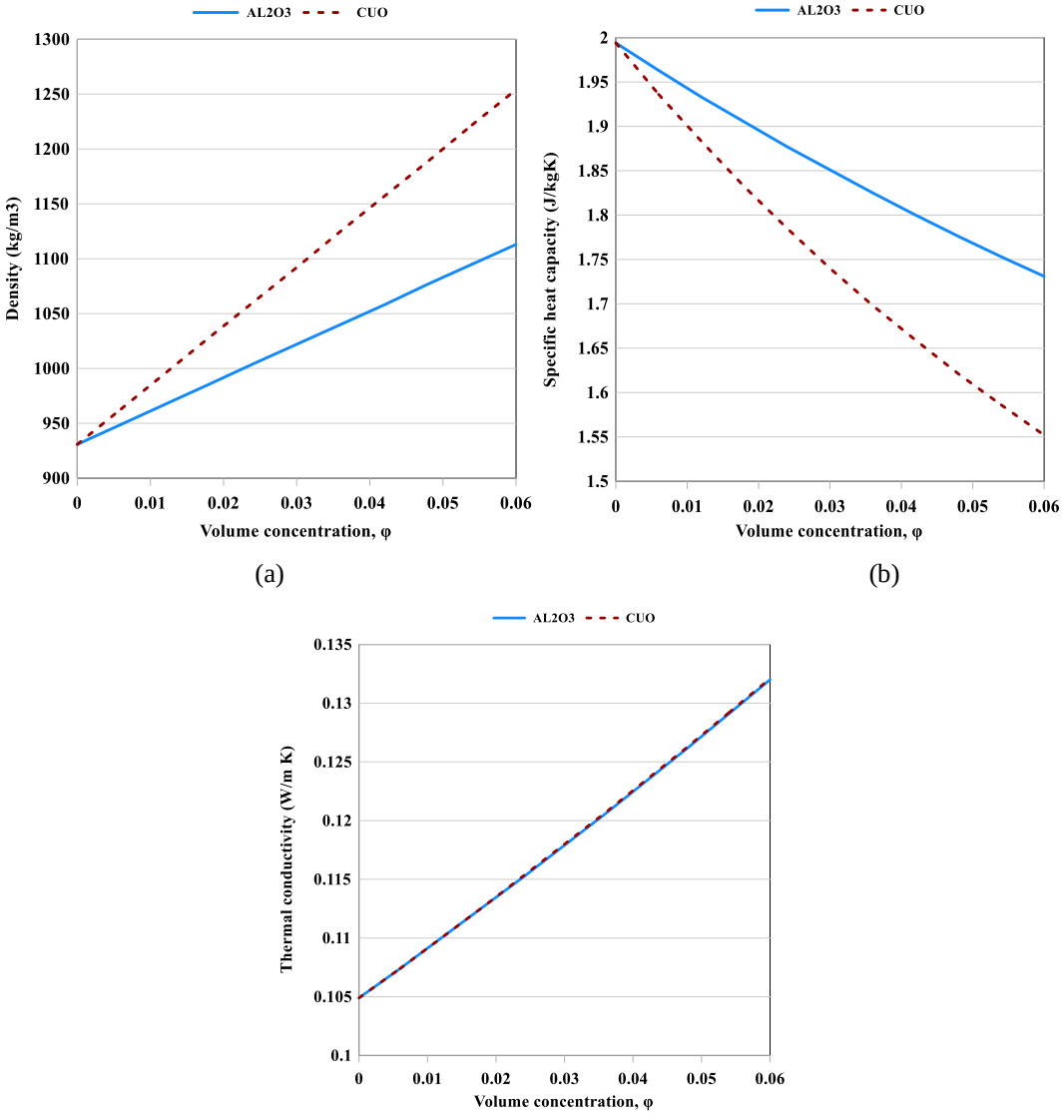

(a) (b)

(c)

Fig. 2. Thermal properties of the studied nanofluids a) density, b) specific heat capacity, c) thermal conductivity

3.3 Parabolic trough collector

By passing through Parabolic trough collectors, the temperature of the geothermal fluid increases, which is calculated by the following equations [54,55]:

$$Q_u = n_{cp} n_{cs} F_R A_{ap} [S - \frac{A_r}{A_{ap}} U_L (T_{r,i} - T_0)] \quad (10)$$

where n_{cp} and n_{cs} are the numbers of collectors in series parallels, respectively. Also, A and F_R are the area and the heat removal factor. Moreover, U_L expresses the total heat loss coefficient of the PTS collector. S is absorbed solar radiation and is defined as:

$$S = G_b \eta_r \quad (11)$$

$$\eta_r = \gamma \tau_c \tau_p \alpha \quad (12)$$

in which γ is the correction factor for diffuse radiation, α is the absorptivity of the

To find F_R and F_l the following equations can be used:

$$F_R = \frac{\dot{m} c_{p,c}}{A_r U_L} [1 - \exp(-\frac{A_r U_L F_l}{\dot{m} c_{p,c}})] \quad (13)$$

$$F_1 = \frac{\frac{1}{U_L}}{\frac{1}{U_L} + \frac{D_{r,0}}{h_{fi}} + (\frac{D_{r,0}}{2k} \ln \frac{D_{r,0}}{D_{r,i}})} \quad (14)$$

where F_l is the collector efficiency factor, h_{fi} is the heat transfer coefficient of the inlet fluid and D is the diameter.

The surface area of PTC is:

$$A_{ap} = (w - D)L \quad (15)$$

in which w is the width and L is the length of the PTC.

Finally, the overall energy efficiency and second law efficiency of the proposed multigeneration system can be defined by the following equations:

receiver, and τ_c and τ_p are the transmissivity of the cover glazing and effective transmissivity of the parabolic trough collector, respectively.

3.4 Exergo-economic analysis

To have a better insight into the overall system efficiency, the exergo-economic analysis should be determined, as the thermodynamic assessment alone is not enough to study the energy systems. The exergo-economic analysis combines concepts of both exergy and economic evaluations and determines the cost per unit of products of the energy conversion system. The general equation for calculating the cost balance for each component can be defined as [56]:

$$\eta_{th,tot} = \frac{\dot{W}_{KAL} + \dot{W}_{ORC-ERC} + \dot{Q}_{cooling} + \dot{Q}_{DWH} + \dot{m}_{53} HHV_{H2} - \dot{W}_{PEM} + \dot{m}_{31} h_{31} - \dot{W}_{RO}}{\dot{Q}_u + \dot{m}_1 h_1} \quad (16)$$

$$\eta_{ex,tot} = \frac{\dot{W}_{KAL} + \dot{W}_{ORC-ERC} + \dot{E}x_{cooling} + \dot{E}x_{53} + \dot{E}x_{54} + \dot{E}x_{51} - \dot{E}x_{50} + \dot{E}x_{31}}{\dot{E}x_{in,sun} + \dot{E}x_1} \quad (17)$$

$$\sum_{out} \dot{C}_{out,k} + C_{w,k} = \sum_{in} \dot{C}_{in,k} + C_{q,k} + Z_k \quad (18)$$

$\dot{C}_{out,k}$: The outlet stream cost rate of components

$C_{w,k}$: The work cost rate

$\dot{C}_{in,k}$: The inlet stream cost rate of components

$C_{q,k}$: The heat transfer cost rate

Z_k indicated the purchase equipment cost rate of each component that can be expressed through the following equation [57]:

$$Z_k = \frac{Z_k \times \varphi \times CRF}{N} \quad (19)$$

φ: the operation and maintenance factor which is assumed as 1.06.

τ: the time operation of the system which is assumed as 8000.

CRF is the capital recovery factor that is defined as [58]:

$$CRF = \frac{i_r (1+i_r)^n}{(1+i_r)^n - 1} \quad (20)$$

in which, i and n are interest and lifetime that are assumed as 12% and 20 years, respectively.

The cost and exergy are related by the specific exergy cost (c_j) which is calculated as:

$$C_j = c_j Ex_j \tag{21}$$

In the exergo-economic analysis, there are some essential parameters such as the average cost per unit exergy of fuel ($c_{f,k}$) and product ($c_{p,k}$), and the exergy destruction cost rate ($C_{D,k}$) which can be defined as follows [59]:

$$c_{f,k} = \frac{C_{f,k}}{Ex_{f,k}} \tag{22}$$

$$c_{p,k} = \frac{C_{p,k}}{Ex_{p,k}} \tag{23}$$

$$C_{D,k} = c_{f,k} \times Ex_{D,k} \tag{24}$$

The exergo-economic factor (f_k) indicates the ratio of the investment cost rate to the summation of investment cost and exergy destruction cost can be calculated as follows [60]:

$$f_k = \frac{Z_k}{Z_k + C_{D,k}} \tag{25}$$

The relative cost difference (r_k) represents the relative increase in the average cost per exergy unit between fuel and product of the component [60]:

$$r_k = \frac{c_{p,k} - c_{f,k}}{c_{f,k}} \tag{26}$$

Table 6 contains the cost functions of each component, which depend on some thermodynamic parameters. For performing the economic analysis, the cost balance is carried out for each element. Moreover, some auxiliary equations are needed to solve the equations. Table 7 includes the cost balance and auxiliary equations of the multigeneration system.

4. Validation

As the proposed multigeneration system is novel, therefore, to certify the accuracy of the modeling, some of the main parts of the system have been validated by previous studies. The results of the RO desalination unit have been compared with the results of Nafey and Sharaf [40] in Table 8. Moreover, Fig. 3 displays the comparison between the results of this study and the work of Zare and Moalemian [65]. According to the table and graphs, a reasonable agreement can be seen between the present modeling and the previous findings.

Table 6. Purchased equipment costs of components [61-64]

Component	Purchase cost ($)
PTC field	$Z_{PTC}=240A_{ap}$
Heat exchangers	$Z_{HX}=130\left(\frac{A}{0.093}\right)^{0.78}$
Evaporator	$Z_{eva}=1397\left(A_{eva}\right)^{0.89}$
Turbine	$Z_t=4405\left(W_t\right)^{0.7}$
Pump	$Z_p=1120\left(W_p\right)^{0.8}$
Expansion valve	$Z_{exv}=114.5\dot{m}_{exv}$
Vapor generator	$Z_{vg}=1397(A)^{0.89}$
Ejector	$Z_{eje}=750\dot{m}_{40}\left(\frac{T_{45}}{P_{45}}\right)^{0.05}\left(P_{40}\right)^{-0.75}$
PEM	$Z_{PEM}=1000\left(W_{pem}\right)$
RO	$Z_{RO}=n_e n_p c_k + n_p c_p + 996(\dot{m}_{31})^{0.8}$

Table 7. The cost balance and auxiliary equations of each component of the proposed system

Component	Cost balance equation	Auxiliary equation
PTC field	$C_{sun}+C_8+Z_{PTC}=C_5$	$c_5=c_8, c_{sun}=0$
Heat exchanger	$C_1+C_7+Z_{HX,geo}=C_2+C_8$	$c_1=5\left\lfloor \frac{\$}{GJ} \right\rfloor, c_1=c_2$
Kalina evaporator	$C_5+C_{29}+Z_{eva,KAL}=C_6+C_9$	$c_5=c_6$
Kalina turbine	$C_9+Z_{t,KAL}=C_{10}+C_{w,t,KAL}$	$c_9=c_{10}$
Kalina recuperator 1	$C_{10}+C_{28}+Z_{re1,KAL}=C_{11}+C_{29}$	$c_{10}=c_{11}, c_{28}=c_{29}$
Kalina recuperator 2	$C_{11}+C_{18}+Z_{re2,KAL}=C_{12}+C_{19}$	$c_{11}=c_{12}, c_{18}=c_{19}$
Kalina recuperator 3	$C_{20}+C_{27}+Z_{re3,KAL}=C_{21}+C_{28}$	$c_{20}=c_{21}, c_{27}=c_{28}$
Kalina recuperator 4	$C_{17}+C_{22}+Z_{re4,KAL}=C_{18}+C_{23}$	$c_{17}=c_{18}, c_{22}=c_{23}$
Kalina mixer 1	$C_{12}+C_{24}+Z_{mx1,KAL}=C_{13}$	-
Kalina mixer 2	$C_{16}+C_{21}+Z_{mx2,KAL}=C_{25}$	-
Kalina condenser 1	$C_{13}=C_{14}+Z_{con1,KAL}$	$c_{13}=c_{14}$
Kalina condenser 2	$C_{25}=Z_{con2,KAL}+C_{26}$	$c_{25}=c_{26}$
Kalina pump 2	$C_{15}=Z_{p2,KAL}+C_{14}+C_{w,p2,KAL}$	$c_{w,p2}=c_{w,t,KAL}$
Kalina pump 3	$C_{27}=Z_{p3,KAL}+C_{26}+C_{w,p3,KAL}$	$c_{w,p3}=c_{w,t,KAL}$
Kalina splitter	$C_{15}+Z_{spl,KAL}=C_{16}+C_{17}$	$c_{16}=c_{17}$
Kalina separator	$C_{19}+Z_{sep,KAL}=C_{20}+C_{22}$	$c_{20}=c_{22}$
Kalina expansion valve 1	$C_{23}+Z_{exv,KAL}=C_{24}$	-
ORC vapor generator	$C_2+C_{35}+Z_{vg,ORC}=C_3+C_{36}$	$c_2=c_3$
ORC turbine	$C_{36}+Z_{t,ORC}=C_{37}+C_{38}+C_{w,t,ORC}$	$c_{36}=c_{37}, c_{36}=c_{38}$
ORC ejector	$C_{37}+C_{45}+Z_{eje,ORC}=C_{39}$	-
ORC preheater	$C_{34}+C_{40}+Z_{prh,ORC}=C_{35}+C_{41}$	$c_{34}=c_{35}$
ORC pump	$C_{34}=Z_{p,ORC}+C_{33}+C_{w,p,ORC}$	$c_{w,p,ORC}=c_{w,t,ORC}$
ORC condenser	$C_{41}+C_{48}+Z_{con,ORC}=C_{42}+C_{49}$	$c_{41}=c_{42}, c_{48}=0$
ORC expansion valve	$C_{43}+Z_{exv,ORC}=C_{44}$	-
ORC evaporator	$C_{44}+C_{46}+Z_{eva,ORC}=C_{45}+C_{47}$	$c_{44}=c_{45}, c_{46}=0$
PEM	$C_{w,PEM}+Z_{PEM}=C_{53}+C_{54}$	$c_{w,PEM}=c_{w,t,ORC}, c_{54}=0$
DWH	$C_{30}+C_{50}+Z_{PEM}=C_4+C_{51}$	$c_3=c_4, c_{50}=0$
RO	$C_{30}+Z_{RO}+C_{w,RO}=C_{31}+C_{32}$	$c_{w,RO}=c_{w,t,KAL}, c_{30}=c_{32}=0$

Table 8. Validation of the simulation results for the RO desalination unit.

Variable	Unit	Present study	Nafey and Sharaf [40]
SPC	kWh/m^3	7.733	7.68
$W_{pump,RO}$	kW	1127	1131
M_f	$\frac{m^3}{h}$	485.8	485.9
M_b	$\frac{m^3}{h}$	340	340.1
X_b	-	0.06418	0.06418
X_d	-	0.000252	0.00025
SR	-	0.9944	0.9944
ΔP	kPa	6871	6850

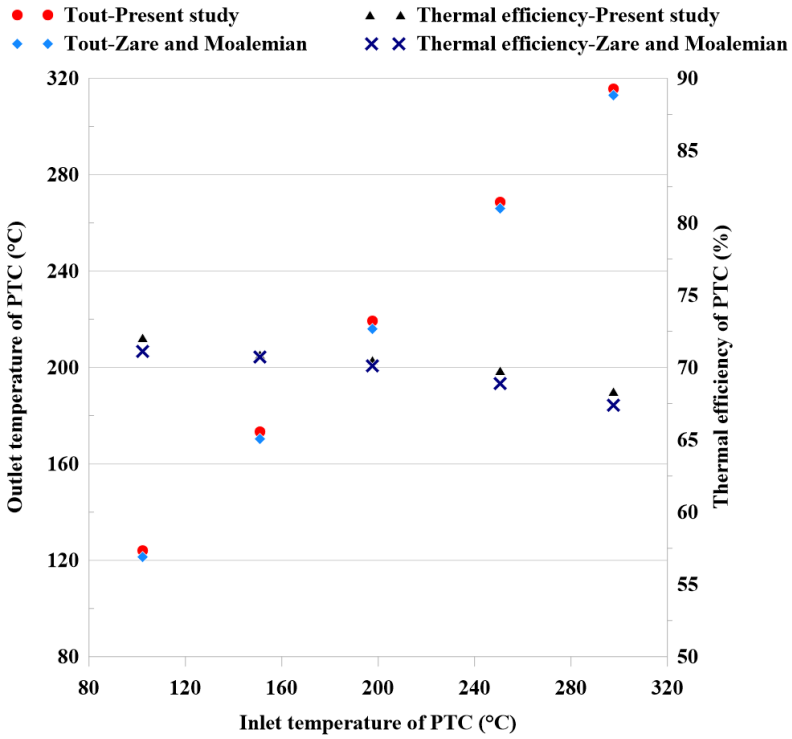

Fig. 3. Comparison of the results of the present work with the results from Zare and Moalemian [65]

5. Results and discussion

After defining all required equations and constants for simulating the solar-geothermal multigeneration system, in the following section, the outputs and results of the studied system assessment are presented through different tables and diagrams and under varying different parameters. Firstly, the overall performance of the proposed system is expressed and then the exergo-economic analysis results are presented. In the end, by parametric analysis, effects of the changing some critical parameters on the outputs of the studied system were investigated. For comparative purposes, the two most common and accessible nanofluids were examined, and then the most desired working fluid for the introduced system was discovered. Fig. 4 summarizes the main steps in conducting the present study. This flow diagram can be helpful to understand the procedure carried out to simulate this system.

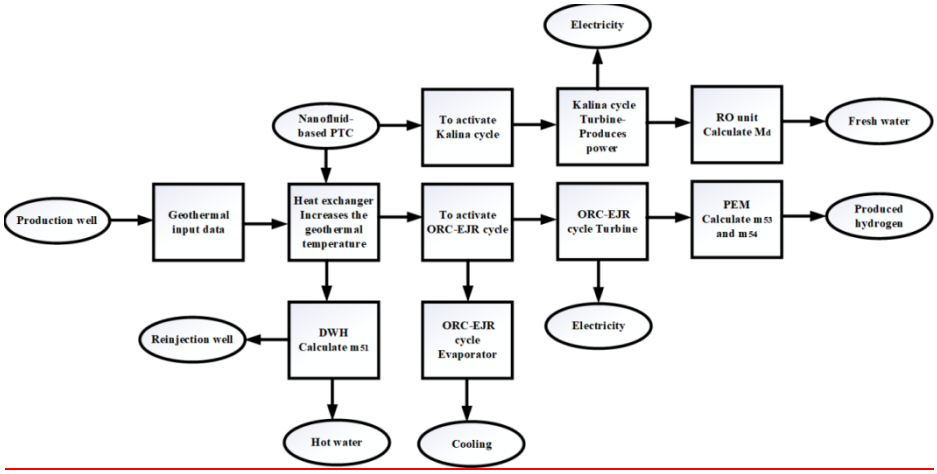

Fig. 4. The flowchart of the pursued procedure in the present study.

5.1.Modeling results

In Table 9, the results of the operational characteristics of the proposed multigeneration system with different collector working fluids are listed and compared from the thermodynamic and cost of the component's point of view. The results show that applying nanofluid improves the performance of the system. Moreover, the comparison proves that CuO-based nanofluid results in the highest solar collector energy and exergy efficiencies, useful solar gained energy, net power output, and the amount of hydrogen produced.

Table 10 displays the quantity of fuel and product exergy, exergy destruction rate, and exergy efficiency of different components. One of the important scales in the exergy analysis of a system is the exergy destruction rate of the components. The results show that the PTC field with 52002 kW has the maximum value of irreversibility. After that, the Kalina evaporator with 5156 kW possesses the second rank in the highest exergy destruction rate. The amount of fuel exergy transformed into product exergy is defined as the exergy efficiency. According to the results, the PTC field shows the lowest exergy efficiency with an amount of 5.92%. The reason is that the PTC converts a large amount of the exergy of solar energy to low-grade energy in the form of a hot working fluid. Kalina condenser and ORC vapor generator have the lowest exergy efficiency after the PTC field which is because of the temperature difference between the fluids which flow inside these components.

Table 9. Thermodynamic performance and cost of components results for the proposed multigeneration system with different collector working fluids

Parameters	Therminol VP1	AL_2O_3 nanofluid	CuO nanofluid
$\eta_{en}(\%)$	33.88	33.89	33.89
$\eta_{ex}(\%)$	16.64	16.67	16.68
$\eta_{en,PTC}(\%)$	67.62	67.82	67.88
$\eta_{ex,PTC}(\%)$	66.44	66.62	66.67
$Q_{u}(kW)$	6260	6279	6284
$Q_{HX,geo}(kW)$	987.8	1007	1012
$Q_{eva,KAL}(kW)$	5332	5333	5333
$W_{net}(kW)$	1366	1369	1370
$Q_{DWH}(kW)$	1362	1365	1365
$m_{Hydrogen}\left(\frac{g}{s}\right)$	0.00164	0.001174	0.001177
$Z(\$)$	142183	142496	142582

Table 10. The quantity of fuel and product exergy, exergy destruction rate, and exergy efficiency of each component of the proposed system.

Component	$Ex_f\,(kW)$	$Ex_p\,(kW)$	$Ex_{D,k}\,(kW)$	$\varepsilon(\%)$
PTC field	55277	3274	52002	5.924
Heat exchanger	367.2	265.9	101.2	72.43
Kalina evaporator	2931	2225	5156	75.94
Kalina turbine	1926	1686	239.5	87.56
Kalina recuperator 1	415.6	212.4	203.2	51.1
Kalina recuperator 2	547.8	236.8	311	43.22
Kalina recuperator 3	20.08	7.29	12.8	36.27
Kalina recuperator 4	64.19	38.13	26.06	59.4
Kalina mixer 1	81887	81882	5.758	100
Kalina mixer 2	40999	40994	5.789	100
Kalina condenser 1	117.3	24.11	93.15	20.56
Kalina condenser 2	44.37	5.847	50.22	13.18
Kalina pump 2	4.56	3.2	1.35	70.28
Kalina pump 3	53.56	37.46	16.1	69.95
Kalina splitter	81768	81768	0	100
Kalina separator	65423	65423	0	100
Kalina expansion valve	40959	40957	1.92	100
ORC vapor generator	617.2	83.76	92.21	13.57
ORC turbine	358.5	297.6	60.87	83.02
ORC ejector	88.99	57.75	31.24	64.9
ORC preheater	46.64	38.36	8.28	82.25
ORC pump	5.01	4.74	0.27	94.61
ORC condenser	104.5	40.44	64.02	38.71
ORC expansion valve	267.5	262.8	4.65	98.26
ORC evaporator	58.87	42.99	15.88	73.02
PEM	298.3	98.44	199.9	33
DWH	199.5	112.4	87.15	56.32
RO	14.61	5.34	9.27	36.57

Table 11. Exergo-economic parameters for different components of the proposed system

Component	$c_{f,k}\left(\frac{\$}{GJ}\right)$	$c_{p,k}\left(\frac{\$}{GJ}\right)$	$Z_k\left(\frac{\$}{h}\right)$	$C_{D,k}\left(\frac{\$}{h}\right)$	$r_k(\%)$	$f_k(\%)$
PTC field	0	0.351	0.131	0	∞	100
Heat exchanger	5	32.09	0.051	0.057	541.8	47.26
Kalina evaporator	0.351	1.76	0.329	0.206	400.9	61.44
Kalina turbine	9.6	43.49	6.262	0.262	353.2	95.98
Kalina recuperator 1	9.6	10.02	0.381	0.384	4.42	49.79
Kalina recuperator 2	9.6	3.57	0.083	0.256	62.81	25.25
Kalina recuperator 3	3.57	7.08	0.05	0.005	98.34	90.67
Kalina recuperator 4	7.41	11.38	0.151	0.022	53.47	87.25
Kalina mixer 1	24.18	24.18	0	0	0	0
Kalina mixer 2	11.93	38.32	0	0	0	0
Kalina condenser 1	24.18	24.18	0.323	0.257	0	55.73
Kalina condenser 2	38.32	38.32	0.194	0.219	0	46.91
Kalina pump 2	43.49	142.6	0.029	0.0067	227.9	81.45
Kalina pump 3	43.49	154.7	0.211	0.08	255.7	72.62
Kalina splitter	24.19	24.19	0	0	0	0
Kalina separator	3.57	3.57	0	0	0	0
Kalina expansion valve	38.75	38.76	0.005	0.008	0	36.72
ORC vapor generator	5	18.48	0.596	0.052	269.6	91.89
ORC turbine	27.01	87.27	1.856	0.187	223.1	90.83
ORC ejector	38.65	30.36	0.0152	0.137	21.44	9.98
ORC preheater	24.61	31.29	0.268	0.023	27.14	92.02
ORC pump	87.27	2.74	0.0009	0.047	96.86	1.85
ORC condenser	24.59	31.46	0.438	0.179	27.95	70.93
ORC expansion valve	31.46	32.07	0.0015	0.0167	1.932	8.23
ORC evaporator	32.07	87.41	0.2	0.058	164.1	77.49
PEM	87.27	263.9	0.00064	1.99	2.024	3.2
DWH	5	20.68	0.151	0.049	313.7	75.27
RO	43.49	72.75	5.095	0.046	67.3	99.11

The results of the exergo-economic analysis of the proposed system are presented in Table 11. Kalina turbine, Ro unit, and ORC turbine have the highest total costs which means the importance of these components from the exergo-economic point of view. PTC field and Kalina turbine have the highest amount of exergoeconomic factors which means that capital and maintenance costs have large shares of these high costs. Moreover, the ORC pump, PEM electrolyzer, and ORC expansion valve have the lowest amounts of exergoeconomic factor which show that the exergy destruction costs dominate the initial investment of these components. The economic investigation shows that the relative cost difference in the heat exchanger is the highest, which means that the average cost per exergy unit of product is superior to the average cost per exergy unit of fuel. Also, it can be inferred that the PEM electrolyzer has the highest exergy destruction cost rate. The reason is that the produced power enters the PEM electrolyzer as an exergy of fuel.

5.2.Parametric study

5.2.1.Effects of Nanoparticles on the performance of the system

By adding nanoparticles to the base fluid, the properties of the base fluid alter. The percentage of nanoparticles is one of the factors that affect the properties of the base fluid considerably and is very decisive in preparing nanofluids. Fig. 5 demonstrates the hydrogen production rate while the nanoparticle percentage varies between 0% and 6%. When the ratio is 0%, both CuO and Al_2O_3-based Therminol_VP1 nanofluids generated 0.001164 g/s amount of hydrogen. According to the graphs, at higher nanoparticle percentages, the hydrogen production rate for the studied nanofluids increased. The reason for the rise is that when the nanoparticle percentage increases, under the defined conditions, the overall production power by the ORC turbine increases, which leads to a rise in the H_2 production rate. The rate of hydrogen production is higher for CuO than for Al_2O_3.

Figure 6 depicts the applying different percentages of CuO and Al_2O_3 nanoparticles to the total net power generated by the proposed system. For both nanofluids, the power production trend is increasing. According to the parametric results, for the range of 0% to 6% of nanoparticles, the power production of CuO-based nanofluid varied from 1366 to 1373, while for Al_2O_3 nanofluid, it increased from 1366 to 1372. It can be seen that the graphs have a stepped behavior. It means that for some percentages of nanofluids, the generated power is steady, while for other amounts, it is rising.

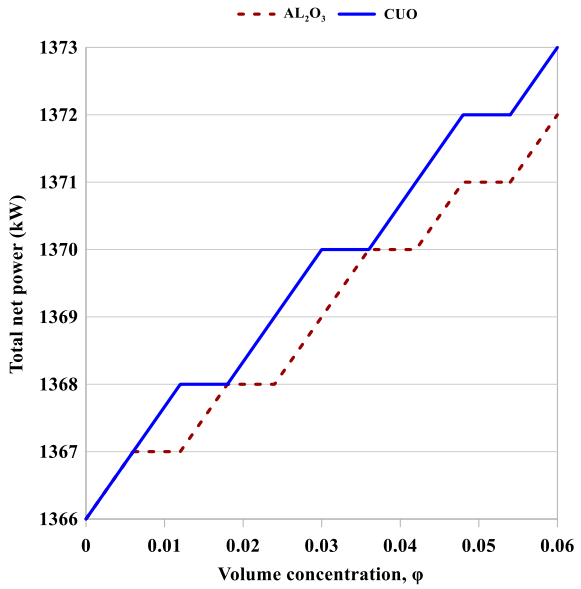

Fig. 5. Effect of nanoparticle percentage on the total net power

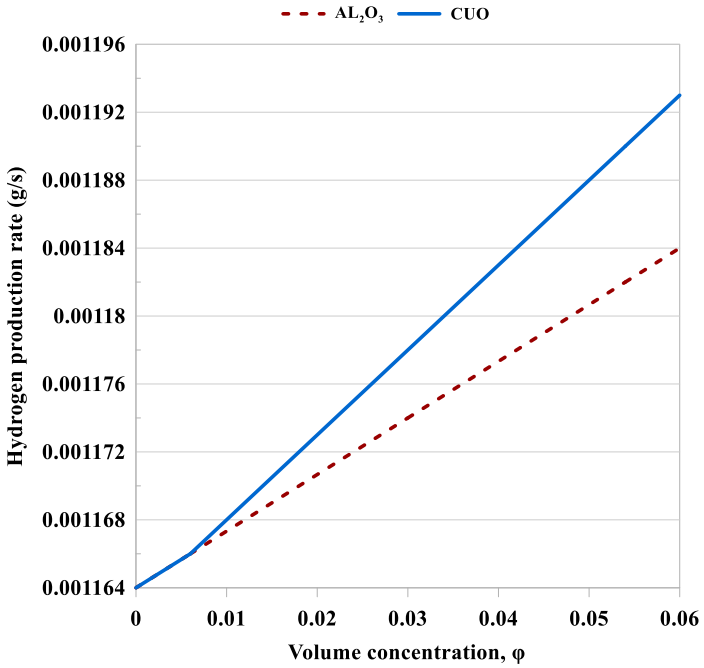

Fig. 6. Effect of nanoparticle percentage on the hydrogen production rate

One of the factors that affect the useful energy gain by the solar collector is the nanoparticle percentage. Fig. 7 illustrates the changes in useful energy gained versus CuO and Al_2O_3 nanoparticles percentage. It is inferred that the nanoparticle percentage increase leads to increased useful energy gained from the PTC. According to equation 10, the nanoparticle concentration change just alters the heat transfer factor. By increasing the nanoparticle concentration, the nanofluid mass flow rate increases while the specific heat transfer reduces. The amount of increase in CuO-based nanofluid is superior to the amount of Al_2O_3 –based nanofluid increase. By altering the ratio from 0 to 0.06, the energy gain rises from 6260 to 6306 kW when CuO-based nanofluid was applied, while when Al_2O_3 –based nanofluid was used, it increased from 6260 to 6290 kW. CuO-based nanofluid compared to the Al_2O_3 –based nanofluid shows better results.

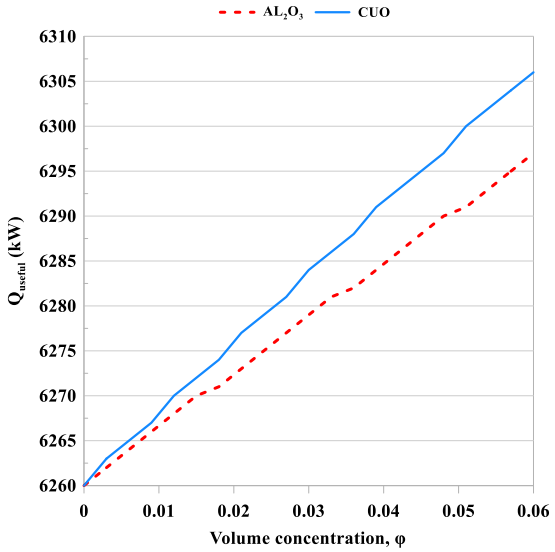

Fig. 7. Effect of nanoparticle percentage on the useful energy achieved from the collector

5.2.2.Effects of solar irradiation on the Performance of the System

Another crucial factor that influences the efficiency of a solar collector is solar irradiation. The amount of energy that passes to the nanofluid in the PTC in the form of temperature is defined as solar irradiance.

Figure 8 demonstrates the trend of useful energy achieved by PTC and the hydrogen production rate when the solar irradiation changes from 400 to 1000 W/m^2 and the nanoparticle percentage is fixed at 0.03. When solar irradiation rises, more energy can transfer to the Kalina cycle which increases the amount of the hydrogen production rate. Moreover, according to equation 10, the absorbed solar radiation (S) rises dramatically and the gained useful energy sharply increases. By investigating the graphs, it is clear that applying two introduced nanofluids has the same impact on the useful energy and hydrogen production rate, but for CuO-based nanofluids, the useful energy is slightly higher. By changing the solar irradiation from 400 to 1000 W/m^2, the CuO-based nanofluid alters from 2845 to 7430 kW, while for the Al_2O_3-based nanofluid, this change is from 2842 to 7424 kW. Finally, for the studied solar irradiation range, both nanofluids increase from 0.00291 to 0.00538 g/s, although in some parts, there is very little difference between the two nanofluids.

The energetic and exergetic efficiencies, as well as the total net power produced by the entire proposed system versus the effect of solar irradiation, are plotted in Fig. 9. There is a negligible difference between the nanofluids applied in this study. Energy and exergy efficiencies of the system decrease with increasing solar irradiation. The amount of reduction in the energetic efficiency is greater than the amount of decline in exergetic efficiency. By increasing solar irradiation, the energetic efficiency of the multigeneration system decreases from 36.77% to 33.26%, while the exergetic efficiency reduces from 17.87% to 16.5%. Moreover, it can be seen that the total net power production increases from 596 to 1638 kW when the solar irradiation changes from 400 to 1000 kW. The reason for the sharp rise in overall power production is that increasing solar irradiation leads to higher solar intensity bouncing back on the receiver, which increases the temperature of the nanofluids leaving the parabolic trough collector. The higher the nanofluid temperature leaving the receiver, the higher the efficiency of the PTC and more power will be produced in the turbines of Kalina and ORC cycles. Finally, more power production will happen, which leads to a higher production of hydrogen rate.

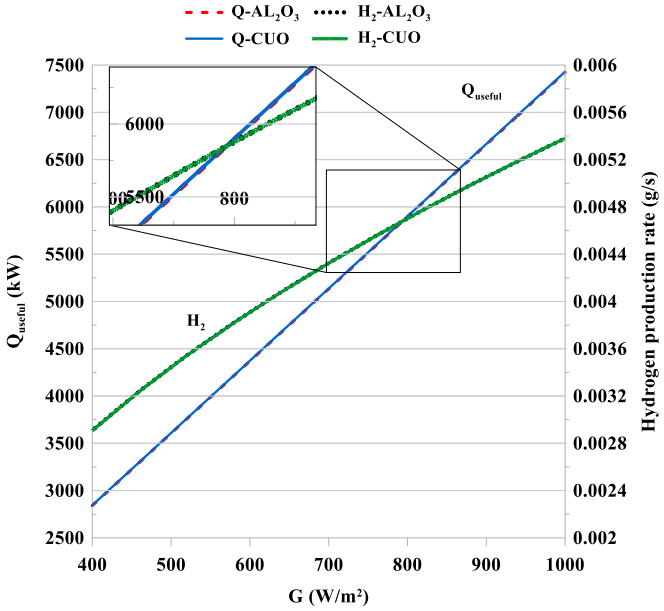

Fig. 8. Effect of solar irradiation on the useful energy achieved from the collector and the hydrogen production rate

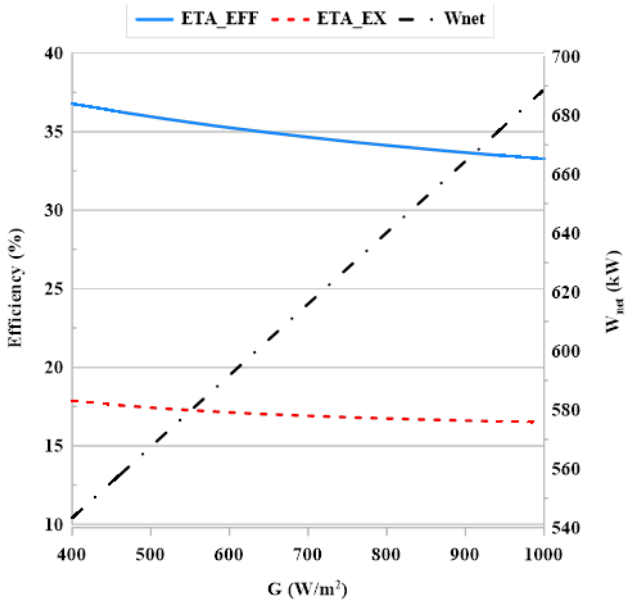

Fig. 9. Effect of solar irradiation on the efficiency and the total net power

The intensity of solar radiation has a considerable impact on the outlet temperature leaving the PTC. The effect of solar irradiance on the outlet temperature of the collector and the heat rate produced by the Kalina cycle evaporator is shown in Fig. 10. The evaluation of the figure makes it clear that for both nanofluids, the outlet temperature rises when the solar radiation intensity increases. Although there is little difference between the studied nanofluids, both nanofluids have the same trends. The outlet temperature of the collector is discovered to be enhanced from 543 K to 688 K by solar irradiance, changing from 400 W/m^2 to 1000 W/m^2. The higher the exit temperature of the solar collector, the higher the heat rate generated by the Kalina cycle evaporator. By increasing the amount of produced heat rate, the power generated by the Kalina cycle will increase too. By varying the solar irradiance, the heat rate generated by the evaporator changes from 1895 kW to 6480 kW.

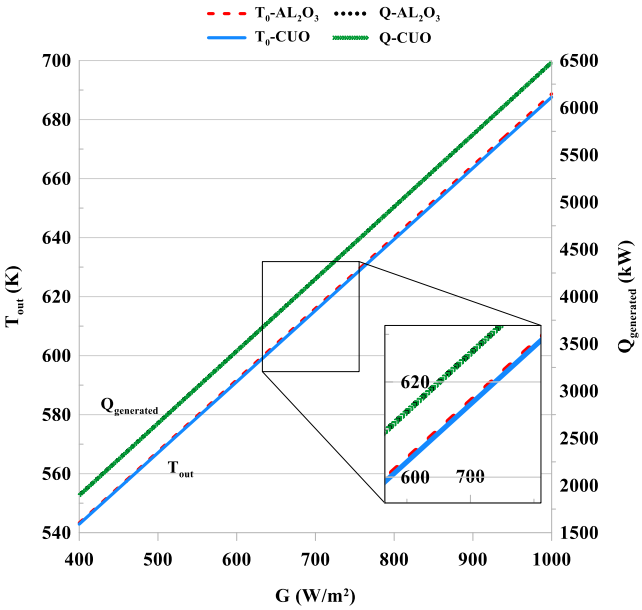

Fig. 10. Effect of solar irradiation on the solar collector outlet temperature and the heat rate produced in the evaporator

5.2.3.Effects of ambient temperature on the performance of the system

To analyze the multigeneration system more comprehensively, the impacts of ambient temperature on the freshwater production rate, total net power generated, and outlet temperature of the collector have been studied.

Figure 11 shows the impact of ambient temperature on the freshwater production rate and total net power generated. For both studied nanofluids, the graphs display a rising trend for freshwater production rate and total net power. By changing ambient temperature from 275 to 325 K, the freshwater production rate varies from 4.867 to 4.898 g/s while generated power alters from 1362 to 1378 kW. As it can be inferred from the charts, it is clear that applying AL_2O_3 or CuO-based nanofluids does not show a remarkable difference, although using CuO as the nanofluid, the system produces a small amount of more net power.

It is evident in Fig. 12 that by enhancing ambient temperature, both collector efficiency and outlet temperature of solar collector go up. By increasing ambient temperature from 275 to 325 K, when AL2O3-based fluid is used, the outlet temperature rises from 651 to 653.5, while for the case of CuO-based nanofluid, the change is from 650.5 to 652.6. Moreover, the effect of ambient temperature change on the collector efficiency is very small, as the collector efficiency for both studied nanofluids varies between 67.5 to 68.25.

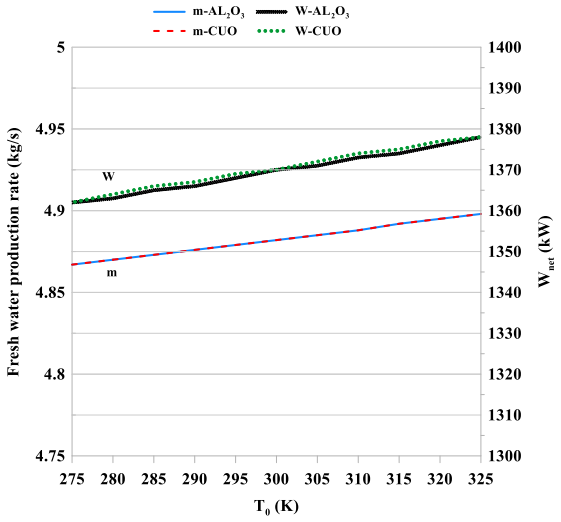

Fig. 11. Effect of ambient temperature on the freshwater production rate and total net power

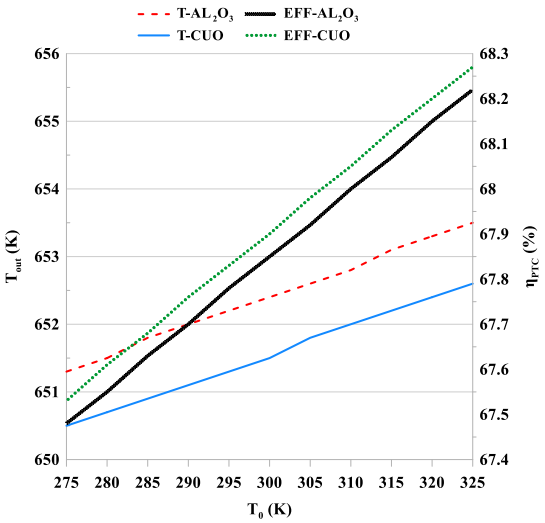

Fig 12. Effect of ambient temperature on the collector outlet temperature and collector efficiency

5.2.4.Effect of solar collector inlet temperature on the performance of the system

The solar collector's inlet temperature is another factor that impacts the efficiency of the multigeneration system. Fig. 13 shows the effect of solar collector inlet temperature on the energy and exergy efficiency of the studied system. The results of the three different cases were investigated, including base fluid (Therminol VP1), AL_2O_3-based nanofluid, and CuO-based nanofluid. As can be inferred from the diagrams, for both energy and exergy efficiencies, nanofluids show higher values compared with base fluid. Among the studied working fluids, CuO offers the best performance. For energetic efficiency, as the inlet temperature increases from 430 K to 490 K, the amount of net power produced by the system increases while the useful energy generated by the solar collector decreases. At first, the amount of energy produced is superior to the produced power and causes a decrease in the thermodynamic efficiency of the system, but then this superiority disappears and causes an increase in the efficiency. For CuO-based nanofluid, the thermal efficiency first decreases from 34.91 % to 33.81 % and then increases to 34.45 %. It can be seen that 470 K is an optimum point for the exergetic efficiency graph. By analyzing the exergetic efficiency graph, it can be concluded that increasing the PTC inlet temperature from 430 K to 490 K, increases the exergy efficiency for all working fluids.

Figure 14 displays the effect of the inlet temperature of the solar collector on the system's hydrogen production rate and freshwater production rate. According to the graphs, when the inlet temperature of the collector increases, the hydrogen production rate decreases while the freshwater production rate increases. By analyzing the results, it can be found that when the inlet temperature rises by about 14%, the freshwater production rate increases by about 18.5%, and the hydrogen production rate decreases by about 70 %. By comparing the graphs, CuO-based nanofluid showed a little better result than AL_2O_3-based nanofluid.

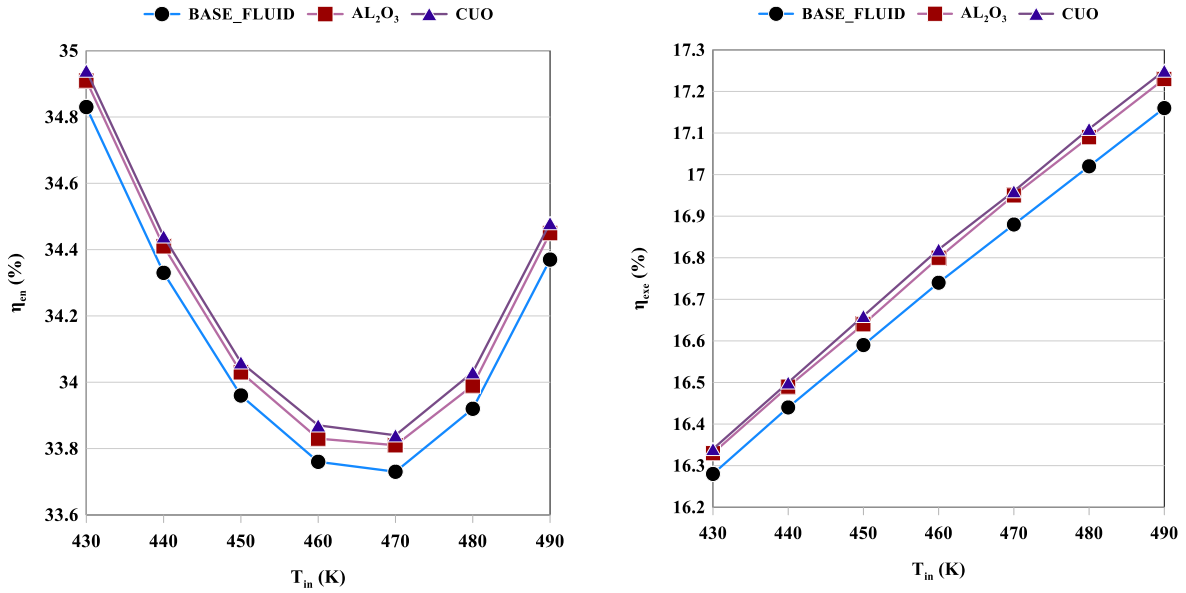

Fig. 13. Effect of collector inlet temperature on the energy and exergy efficiency

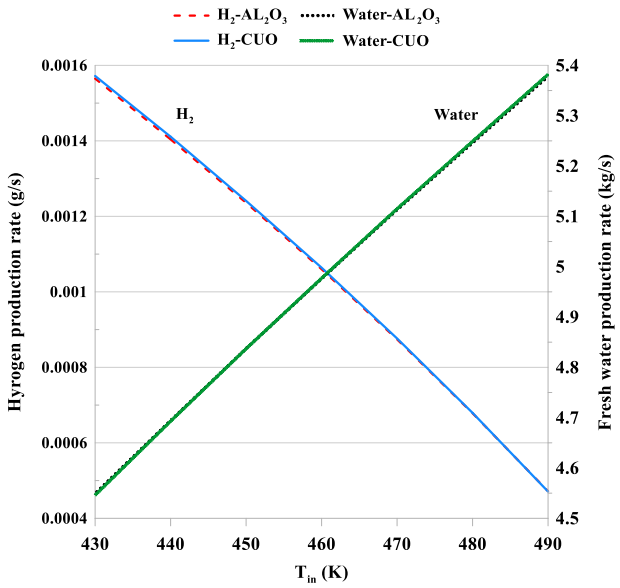

Fig. 14. Effect of collector inlet temperature on the hydrogen and freshwater production rates

6. Conclusions

In the present study, a multigeneration system was investigated in which solar and geothermal energies, as the two plentiful and clean sources of energy, are combined to satisfy the required demands of an area. To better understand the studied system, energy, and exergy research was performed. A comparative investigation among the base fluid and two introduced nanofluids was done to find the most suitable working fluid for the solar collector.

Some of the main conclusions are as follows:

- Although comparing Al_2O_3-based and CuO-based nanofluids show almost the same results, in general, it can be concluded that CuO-based nanofluid shows better results.
- Compared to the Therminol VP1 as the base fluids, applying nanofluids leads to higher power production and better efficiency.
- It was concluded that the hydrogen production rate for CuO nanofluid is higher than Al_2O_3 nanofluid when the nanoparticle concentration increases gradually.
- The results showed that by varying nanoparticle percentage, total net power produced and useful energy achieved from the collector has a rising trend, and CuO-based nanofluid showed higher amounts.
- By changing the solar irradiation from 400 to 1000 (W/m^2), the total net power produced, hydrogen production rate, useful energy achieved from the collector, solar collector outlet temperature, and heat rate produced in the solar evaporator increased while the total energy and exergy efficiency of the system decreased.
- Ambient temperature is one of the factors that affect the performance of the studied multigeneration system. While the ambient temperature changes from 275 to 325 K, all the studied parameters, including freshwater production rate, total net power, collector efficiency, and collector outlet temperature, tend to increase.
- When the collector inlet temperature varies between 430 to 490 K, the energy efficiency of the proposed system first tends to decrease, but at 470 K, it starts increasing. For exergy efficiency, a rising trend can be seen. Moreover, by increasing inlet temperature, the hydrogen production rate decreases while the freshwater production rate increases.

References

[1] Abdolalipouradl, M., Mohammadkhani, F., Khalilarya, S. and Yari, M., Thermodynamic and exergoeconomic analysis of two novel tri-generation cycles for power, hydrogen and freshwater production from geothermal energy. Energy Conversion and Management (2020) 226:113544.

[2] Keshavarzzadeh, A.H., Ahmadi, P. and Safaei, M.R., Assessment and optimization of an integrated energy system with electrolysis and fuel cells for electricity, cooling and hydrogen production using various optimization techniques. International Journal of Hydrogen Energy (2019) 44:21379-21396.

[3] Ahmadi P, Dincer I, Rosen MA. Thermodynamic modeling and multi-objective evolutionary-based optimization of a new multigeneration energy system. Energy Conversion and Management (2013) 76:282 300.

[4] Taheri M, Mosaffa A, Farshi LG. Energy, exergy and economic assessments of a novel integrated biomass based multigeneration energy system with hydrogen production and LNG regasification cycle. Energy (2017) 125:162-177.

[5] Al-Ali, M. and Dincer, I. Energetic and exergetic studies of a multigenerational solar–geothermal system. Applied Thermal Engineering (2014) 71:16-23.

[6] Panchal, S., Dincer, I. and Agelin-Chaab, M. Analysis and evaluation of a new renewable energy based integrated system for residential applications. Energy and Buildings (2016) 128:900-910.

[7] Khalid, F., Dincer, I. and Rosen, M.A. Techno-economic assessment of a solar-geothermal multigeneration system for buildings. International Journal of Hydrogen Energy (2017) 42:21454-21462.

[8] Waseem, S., Ratlamwala, T.A.H., Salman, Y. and Bham, A.A. Geothermal and solar based multigenerational system: a comparative analysis. International Journal of Hydrogen Energy (2020) 45:5636-5652.

[9] Li, T., Qin, H., Wang, J., Gao, X., Meng, N., Jia, Y. and Liu, Q. Energetic and exergetic performance of a novel polygeneration energy system driven by geothermal energy and solar energy for power, hydrogen and domestic hot water. Renewable Energy (2021) 175:318-336.

[10] Sen, O., Guler, O.F., Yilmaz, C. and Kanoglu, M. Thermodynamic modeling and analysis of a solar and geothermal assisted multi-generation energy system. Energy Conversion and Management (2021) 239:114186.

[11] Atiz, A. Comparison of three different solar collectors integrated with geothermal source for electricity and hydrogen production. International Journal of Hydrogen Energy (2020) 45:31651-31666.

[12] Sohani, A., Delfani, F., Hosseini, M., Sayyaadi, H., Karimi, N., Li, L.K. and Doranehgard, M.H. Price inflation effects on a solar-geothermal system for combined production of hydrogen, power, freshwater and heat. International Journal of Hydrogen Energy (2022)

[13] Ghorbani, B., Mehrpooya, M. and Sadeghzadeh, M. Process development of a solar-assisted multi-production plant: power, cooling, and hydrogen. International Journal of Hydrogen Energy (2020) 45:30056-30079.

[14] Mahmoudan, A., Esmaeilion, F., Hoseinzadeh, S., Soltani, M., Ahmadi, P. and Rosen, M. A geothermal and solar-based multigeneration system integrated with a TEG unit: Development, 3E analyses, and multi-objective optimization. Applied Energy (2022) 308,118399.

[15] Hashemian, N. and Noorpoor, A. A geothermal-biomass powered multi-generation plant with freshwater and hydrogen generation options: Thermo-economic-environmental appraisals and multi-criteria optimization. Renewable Energy (2022) 198:254.

[16] Bellos E, Tzivanidis C, Tsimpoukis D. Thermal, hydraulic and exergetic evaluation of a parabolic trough collector operating with thermal oil and molten salt based nanofluids. Energy Conversion and Management (2018) 156:388–402.

[17] Fuqiang W, Ziming C, Jianyu T, Yuan Y, Yong S, Linhua L. Progress in concentrated solar power technology with parabolic

trough collector system: A comprehensive review. Renewable Sustainable Energy Review (2017) 79:1314–28.

[18] Subramani J, Nagarajan PK, Wongwises S, El-Agouz SA, Sathyamurthya R. Experimental Study on the Thermal Performance and Heat Transfer Characteristics of Solar Parabolic Trough Collector Using Al_2O_3 Nanofluids. Environmental Program Sustainable Energy (2018) 37:1149–59.

[19] Mwesigye A, Huan Z, Meyer JP. Thermodynamic optimisation of the performance of a parabolic trough receiver using synthetic oil– Al_2O_3 nanofluid. Applied Energy (2015) 156:398–412.

[20] Bellos E, Tzivanidis C, Antonopoulos KA, Gkinis G. Thermal enhancement of solar parabolic trough collectors by using nanofluids and converging-diverging absorber tube. Renewable Energy (2016) 94:213–22.

[21] Wang Y, Xu J, Liu Q, Chen Y, Liu H. Performance analysis of a parabolic trough solar collector using Al_2O_3/synthetic oil nanofluid. Appl Thermal Engineering (2016) 107:469–78.

[22] Abid, M., Ratlamwala, T.A. and Atikol, U. Solar assisted multi-generation system using nanofluids: a comparative analysis. International Journal of Hydrogen Energy (2017) 42, 21429-21442.

[23] Ratlamwala, T.A.H., Waseem, S., Salman, Y. and Bham, A.A. Geothermal and solar energy–based multigeneration system for a district. International Journal of Energy Research (2019) 43:5230-5251.

[24] Bellos, E., Tzivanidis, C. and Said, Z. A systematic parametric thermal analysis of nanofluid-based parabolic trough solar collectors. Sustainable Energy Technologies and Assessments (2020) 39:100714.

[25] Khan, M.S., Amber, K.P., Ali, H.M., Abid, M., Ratlamwala, T.A. and Javed, S. Performance analysis of solar assisted multigenerational system using therminol VP1 based nanofluids: a comparative study. Thermal Science (2020) 24:865-878.

[26] Ibrahim, A. and Kayfeci, M. Comparative analysis of a solar trigeneration system based on parabolic trough collectors using graphene and ferrofluid nanoparticles. Thermal Science, (2020) 25:2549-2563.

[27] Allouhi, A., Amine, M.B., Saidur, R., Kousksou, T. and Jamil, A. Energy and exergy analyses of a parabolic trough collector operated with nanofluids for medium and high temperature applications. Energy Conversion and Management (2018) 155:201-217.

[28] Kalbande, V.P., Walke, P.V. and Rambhad, K. Performance of oil-based thermal storage system with parabolic trough solar collector using Al2O3 and soybean oil nanofluid. International Journal of Energy Research (2021) 45:15338-15359.

[29] Tonekaboni N., Salarian H., Nimvari M.E. and Khaleghinia J. Energy and exergy analysis of an enhanced solar CCHP system with a collector embedded by porous media and nano fluid. Journal of Thermal Engineering (2021) 7:1489-1505.

[30] Said, Z., Ghodbane, M., Boumeddane, B., Tiwari, A.K., Sundar, L.S., Li, C., Aslfattahi, N. and Bellos, E. Energy, exergy, economic and environmental (4E) analysis of a parabolic trough solar collector using MXene based silicone oil nanofluids. Solar Energy Materials and Solar Cells (2022) 239:111633.

[31] EES. Engineering equation solver, (2018).

[32] Bassetti, M.C., Consoli, D., Manente, G. and Lazzaretto, A. Design and off-design models of a hybrid geothermal-solar power plant enhanced by a thermal storage. Renewable Energy (2018) 128: 460-472.

[33] Musharavati, F., Khanmohammadi, S. and Pakseresht, A. A novel multi-generation energy system based on geothermal energy source: Thermo-economic evaluation and optimization. Energy Conversion and Management (2021) 230:113829.

[34] Alirahmi, S.M., Rostami, M. and Farajollahi, A.H. Multi-criteria design optimization and thermodynamic analysis of a novel multi-generation energy system for hydrogen, cooling, heating, power, and freshwater. International Journal of Hydrogen Energy (2020) 45:15047-15062.

[35] Al-Hamed, K.H.M. and Dincer, I. Investigation of a concentrated solar-geothermal integrated system with a

combined ejector-absorption refrigeration cycle for a small community. International Journal of Refrigeration (2019) 106:407-426.

[36] Al-Sulaiman, F.A. Exergy analysis of parabolic trough solar collectors integrated with combined steam and organic Rankine cycles. Energy Conversion and Management (2013) 77:441–449.

[37] Alirahmi, S.M., Rahmani Dabbagh, S., Ahmadi, P., Wongwises, S. Multi-objective design optimization of a multi-generation energy system based on geothermal and solar energy. Energy Conversion and Management (2020) 205:112426.

[38] Singh, H. and Mishra, R.S. Performance analysis of solar parabolic trough collectors driven combined supercritical CO2 and organic Rankine cycle. Engineering Science and Technology, an International Journal (2018) 21: 451-464.

[39] Sarabchi, N., Mahmoudi, S.S., Yari, M. and Farzi, A. Exergoeconomic analysis and optimization of a novel hybrid cogeneration system: High-temperature proton exchange membrane fuel cell/Kalina cycle, driven by solar energy. Energy Conversion and Management (2019) 190:14-33.

[40] Nafey A.S, Sharaf M.A. Combined solar organic Rankine cycle with reverse osmosis desalination process: energy, exergy, and cost evaluations. Renewable Energy (2010) 35:2571-80.

[41] Nemati, A., Sadeghi, M., Yari, M. Exergoeconomic analysis and multi-objective optimization of a marine engine waste heat driven RO desalination system integrated with an organic Rankine cycle using zeotropic working fluid. Desalination (2017) 422:113–.

[42] Habibzadeh, A., Rashidi, M.M. and Galanis, N. Analysis of a combined power and ejector-refrigeration cycle using low temperature heat. Energy Conversion and Management (2013) 65:381-391.

[43] Aliahmadi, M., Moosavi, A. and Sadrhosseini, H. Multi-objective optimization of regenerative ORC system integrated with thermoelectric generators for low-temperature waste heat recovery. Energy Reports (2021) 7:300-313.

[44] Takleh, H.R. and Zare, V. Proposal and thermoeconomic evaluation with reliability considerations of geothermal driven trigeneration systems with independent operations for summer and winter. International Journal of Refrigeration (2021) 127:34-46.

[45] Xi, Z., Eshaghi, S. and Sardari, F. Energy, exergy, and exergoeconomic analysis of a polygeneration system driven by solar energy with a thermal energy storage tank for power, heating, and freshwater production. Journal of Energy Storage (2021) 36: 102429.

[46] Khodadadi F., Deymi-Dashtebayaz M. and Lakzian E. Parametric analysis of combined power and freshwater producing system for natural gas engine heat recovery. Energy Conversion and Management (2020) 225:113464.

[47] Abdolalipouradl M, Khalilarya S, Jafarmadar S. Energy and exergy analysis of a new power, heating, oxygen and hydrogen cogeneration cycle based on the Sabalan Geothermal Wells. International Journal of Engineering (2019) 32:445–50.

[48] Ghasemi S.E. and Ranjbar A.A. Thermal performance analysis of solar parabolic trough collector using nanofluid as working fluid: a CFD modelling study. Journal of Molecular Liquids (2016) 222:159-166.

[49] Kasaeian, A.B. Convection heat transfer modeling of Ag nanofluid using different viscosity theories. IIUM Engineering Journal (2012) 13:1-11.

[50] Khanafer, K. and Vafai, K. A critical synthesis of thermophysical characteristics of nanofluids. International journal of heat and mass transfer (2011) 54:4410-4428.

[51] Yu, W. and Choi, S.U.S. The role of interfacial layers in the enhanced thermal conductivity of nanofluids: a renovated Maxwell model. Journal of nanoparticle research (2003) 5:167-171. [52] Duangthongsuk, W. and Wongwises, S. An experimental study on the heat transfer performance and pressure drop of TiO2-water nanofluids flowing under a turbulent flow regime. International Journal of Heat and Mass Transfer (2010) 53:334-344.

[53] Batchelor, G.K., 1977. The effect of Brownian motion on the bulk stress in a

suspension of spherical particles. Journal of fluid mechanics (1977) 83:97-117.
[54] Kalogirou, S.A.Solar energy engineering: processes and systems. Academic Press, (2013)
[55] Yüksel, Y.E. Thermodynamic assessment of modified Organic Rankine Cycle integrated with parabolic trough collector for hydrogen production. International Journal of Hydrogen Energy (2018) 43:5832-5841.
[56] Bejan A, Tsatsaronis G, Moran M. Thermal design and optimization. John Wiley & Sons; 1995.
[57] Assareh, E., Alirahmi, S.M. and Ahmadi, P. A Sustainable model for the integration of solar and geothermal energy boosted with thermoelectric generators (TEGs) for electricity, cooling and desalination purpose. Geothermics (2021) 92:102042.
[58] Yu, Z., Su, R. and Feng, C. Thermodynamic analysis and multi-objective optimization of a novel power generation system driven by geothermal energy. Energy (2020) 199:117381.
[59] Mohammadkhani, F., Yari, M. and Ranjbar, F. A zero-dimensional model for simulation of a Diesel engine and exergoeconomic analysis of waste heat recovery from its exhaust and coolant employing a high-temperature Kalina cycle. Energy Conversion and Management (2019) 198:111782.
[60] Boyaghchi, F.A. and Chavoshi, M. Multi-criteria optimization of a micro solar-geothermal CCHP system applying water/CuO nanofluid based on exergy, exergoeconomic and exergoenvironmental concepts. Applied Thermal Engineering (2017) 112:660-675.
[61] Khosravi, A., Koury, R.N.N. and Machado, L., 2018. Thermo-economic analysis and sizing of the components of an ejector expansion refrigeration system. International Journal of Refrigeration, 86, pp.463-479.
[62] Kianfard, H., Khalilarya, S. and Jafarmadar, S. Exergy and exergoeconomic evaluation of hydrogen and distilled water production via combination of PEM electrolyzer, RO desalination unit and geothermal driven dual fluid ORC. Energy conversion and management (2018) 177:339-349.
[63] Ahmadi, P., Dincer, I. and Rosen, M.A., 2014. Multi-objective optimization of a novel solar-based multigeneration energy system. Solar Energy, 108, pp.576-591.
[64] Malik, M.Z., Musharavati, F., Khanmohammadi, S., Pakseresht, A.H., Khanmohammadi, S. and Nguyen, D.D., 2020. Design and comparative exergy and exergo-economic analyses of a novel integrated Kalina cycle improved with fuel cell and thermoelectric module. Energy Conversion and Management, 220, p.113081.
[65] Zare, V., Moalemian, A.J.E.C. Parabolic trough solar collectors integrated with a Kalina cycle for high temperature applications: Energy, exergy and economic analyses. Energy Conversion and Management (2017) 151:681-692.